

Scaling law for Kasha’s rule in photoexcited subwavelength molecular aggregates

R. Holzinger,¹ N. S. Bassler,^{2,3} H. Ritsch,¹ and C. Genes^{2,3}

¹*Institut für Theoretische Physik, Universität Innsbruck,
Technikerstrasse 21a, A-6020 Innsbruck, Austria*

²*Max Planck Institute for the Science of Light, Staudtstraße 2, D-91058 Erlangen, Germany*

³*Department of Physics, Friedrich-Alexander-Universität Erlangen-Nürnberg, Staudtstraße 7, D-91058 Erlangen, Germany*

(Dated: April 21, 2023)

We study the photophysics of molecular aggregates from a quantum optics perspective, with emphasis on deriving scaling laws for the fast non-radiative relaxation of collective electronic excitations, referred to as Kasha’s rule. At deep subwavelength separations, quantum emitter arrays exhibit an energetically broad manifold of collective states with delocalized electronic excitations originating from near field dipole-dipole exchanges between the aggregate’s monomers. Photoexcitation with visible light addresses almost exclusively symmetric collective states, which for an arrangement known as H-aggregate, have the highest energies (hypsochromic shift). The extremely fast subsequent non-radiative relaxation via intramolecular vibrational modes then populates lower energy, subradiant states which results in the effective inhibition of fluorescence. Our treatment allows for the derivation of an approximate linear scaling law of this relaxation process with the number of available low energy vibrational modes and reveals its direct proportionality to the dipole-dipole interaction strength between neighbouring monomers.

I. INTRODUCTION

Molecular aggregates [1–3] are self-ordered arrangements of monomers with a strong optical transition dipole strength. Owing to the dense packing of monomers within the aggregate, at the level of tens of nanometers, thus much below an optical wavelength and despite inhomogeneous broadening and separation disorder, they exhibit delocalized excitons [4]. This allows strong coupling to external light modes, resulting in collectively modified fluorescence rates. Following the discovery of J- and H-aggregates in the 1930s by Scheibe [5] and Jelley [6] their standard understanding is based on the original approach introduced by Kasha in the 1960s [7]. Currently, J-aggregates are widely employed in light-matter coupling experiments aiming at the modification of material properties via the manipulation of the electromagnetic vacuum mode density around electronic resonances [8].

In quantum optics, there is a growing interest in the cooperative behavior of subwavelength matter systems [9], confined to regions comparable to the typical wavelength λ of visible light. Implementation platforms include synthetic systems such as atoms in optical lattices, vacancy centers, quantum dots, etc., strongly building on the seminal work of Dicke [10] in the 1950s. Dicke predicted that the rate of radiative emission from indistinguishable electronic systems, such as a number \mathcal{N} of atoms placed within a volume much smaller than λ^3 , scales quadratically with particle number \mathcal{N} . This phenomenon, called Dicke superradiance [11, 12], is accompanied by the closely related effect of subradiance, where the emission rate of collective states can be much lower than that of an isolated single quantum emitter [13]. Subradiance holds many promises towards applications of robust quantum state design or in quantum metrology and sensing [9, 14]. Moreover, the open system dynamics combined with the study of naturally occurring photosynthetic systems have

triggered many investigations into providing design principles of subwavelength biomimetic systems [15–18].

Such cooperative behavior can also be naturally studied in molecular aggregates even at room temperature [18]. First, their small overall dimensions means that under external illumination the light-matter interaction strength is collectively enhanced by a factor $\sqrt{\mathcal{N}}$ - the number of monomers, due to the increase in the oscillator strength. The symmetric superposition of the individual electronic excitation states exhibits the lowest energy for a head-to-tail arrangement, i.e. a J-aggregate [1]. Consequently, the symmetric state is protected against further vibrational relaxation and hence the J-aggregate’s fluorescence is strongly increased. For the opposite case of parallel arrangement of the dipole moments (H-aggregate), i.e. the side-by-side configuration, fluorescence is inhibited due to vibrational relaxation to subradiant lower energy states. These states deplete the symmetric state, in this case situated on top of the energy band, in a process generally denoted as Kasha’s rule. Consequently, fluorescence is decreased and the system can undergo other processes such as the singlet to triplet transition followed by intersystem crossing and subsequently radiative relaxation via phosphorescence. At close distances, not only the radiative emission is modified but the inherent near-field dipole-dipole interactions lead to observable energy shifts in the absorption peak tied to the symmetric state. It is shifted towards higher energies (bathochromic) for H-aggregates and to lower energy (hypsochromic) for J-aggregates when compared to the bare monomer’s absorption peak [1, 3].

To shed some new light into some of these phenomena we follow here a quantum optics inspired approach [19] to analyse the photophysics of molecular aggregates. The aim is to provide an analytical description of Kasha’s rule taking into account dipole-dipole interactions, electron-vibron couplings and vibrational relaxation. Our treatment involves a formulation where \mathcal{N} monomers in a linear

chain configuration with separation d form an aggregate, as depicted in Fig. 1(a). Each monomer is described as a two level electronic quantum emitter with an intrinsic coupling to a number n of vibrational degrees of freedom (see Fig. 1(b)). The near-field dipole-dipole couplings between monomers leads to the possibility of excitation migration within the whole aggregate and thus to the creation of delocalized excitons. We characterize these delocalized states by their collective energy shifts, seen as an energy dispersion curve in Fig. 1(c) and by their radiative properties. Notice that for such small separations, the light cone basically includes a single state characterized by a quasi-momentum $q = 0$ (the symmetric superposition) while all other states fall outside this light cone [14]. Uniform illumination leads to the activation of the symmetric electronic superposition, which in turn can indirectly redistribute energy to a manifold of asymmetric, dark collective states. In the specific case of H-aggregates, the higher energetic symmetric state relaxes quickly via vibronically-aided processes to the bottom asymmetric states characterized by subradiance. This presents an effective reduction of fluorescence, thus favoring transitions to triplet states and thus phosphorescence. The mechanism is roughly depicted in Fig. 1(c) as the initial excitation slides down quickly to the bottom of the dispersion curve. Snapshots of this process in time are shown in Fig. 1(d) describing the time evolution of the excitation from the symmetric, quickly decaying collective state to the bottom asymmetric, robust electronic states. A perturbative treatment allows us to derive an analytical expression for this rate, revealing independence of the number of monomers and a linear scaling with the number of nuclear vibrations available for the dissipation of electronic energy into low energy vibrations. Moreover, the timescale of the process is set by the strength of the nearest neighbor dipole-dipole interaction.

The manuscript is structured as follows: we first introduce the model for \mathcal{N} coupled molecular quantum emitters in Sec. II. We then quickly review the transformation from the bare monomer basis to the collective aggregate basis as introduced formally in Ref. [20]. In Sec. III we derive rate equations for collective state populations and compare with numerical simulation for the specific case of H-aggregates.

II. MODEL

We consider a deep subwavelength ensemble of molecular quantum emitters in an equidistant chain configuration (see Fig. 1(a)) mimicking a molecular aggregate comprised of \mathcal{N} identical monomers and with a typical inter-monomer distance d in the nm range. As photoexcitation is performed with light sources of wavelength $2\pi/k_0$ (with k_0 the wavevector) in the μm range, the condition $k_0d \ll 1$ is fulfilled. Each monomer is assumed to undergo a single electronic transition which in turn is coupled to a n vibrational

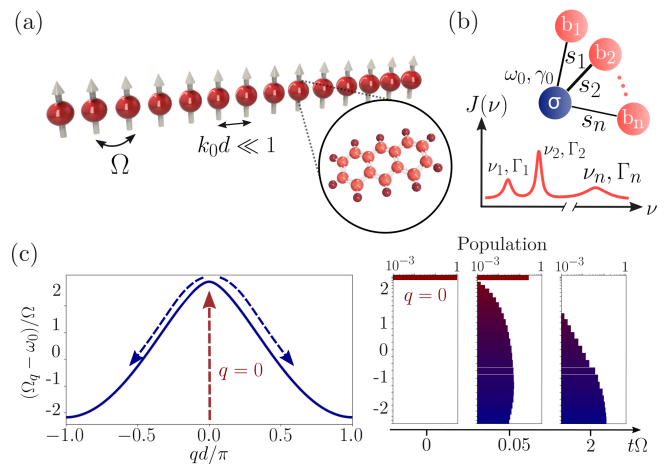


FIG. 1. (a) Illustration of a tail-to-tail arrangement of monomer dipoles (H-aggregate configuration). With separations in the nm range, the condition $k_0d \ll 1$ is fulfilled leading to strong near-field dipole-dipole interactions with nearest-neighbour strengths Ω . (b) Diagram describing electron-vibron interactions within each monomer. A single electronic transition operator σ is coupled to n vibrational mode operators b_m with frequencies ν_m , linewidths Γ_m and Huang-Rhys factors s_m , where m runs from 1 to n . (c) Energy band diagram for a mesoscopic chain as a function of the quasi-momentum q . Upon photoexcitation, only the symmetric state ($q = 0$) is initially populated. Subsequently, an almost instantaneous relaxation towards lower energy states takes place. On the right side, the population distribution of the collective excitation modes for $k_0d = 0.0126$ is presented in snapshots at different times, showing that the electron-vibron coupling combined with vibrational relaxation leads to the migration of energy towards the lowest energy asymmetric modes. We have considered a large n spanning the range of frequencies from 0 to 4Ω , with $\Gamma_m = \nu_m/10$ and identical $s_m = 10^{-2}$.

modes. Each vibrational mode has a frequency ν_m and relaxation rate Γ_m , where m runs from 1 to n . The monomer can undergo spontaneous emission at rate γ_0 , owing to the coupling to the electromagnetic environment.

Electron-vibron interactions - For each monomer j , the electronic transition is at frequency splitting ω_0 ($\hbar = 1$) and is described by the collapse operator $\sigma_j = |g\rangle_j \langle e|_j$. The vibrational degrees of freedom are described by bosonic operators b_{jm} satisfying the commutation relations $[b_{jm}, b_{j'm'}^\dagger] = \delta_{jj'}\delta_{mm'}$. The vibronic couplings are illustrated in Fig. 1(b) as links between the electronic and vibration operators with magnitude characterized by the Huang-Rhys factors s_m . The electronic and vibrational degrees of freedom are subject to loss quantified by the spontaneous emission rate γ_0 and by the vibrational relaxation rates Γ_m , respectively. The Hamiltonian for all \mathcal{N} monomers is obtained as a sum

over each particle's Hamiltonian

$$h^{(j)} = \bar{\omega}_0 \sigma_j^\dagger \sigma_j + \sum_{m=1}^n \nu_m \left(b_{jm}^\dagger b_{jm} - \sqrt{s_m} \sigma_j^\dagger \sigma_j (b_{jm}^\dagger + b_{jm}) \right). \quad (1)$$

Notice that the bare frequency is Stokes shifted $\bar{\omega}_0 = \omega_0 + \sum_m s_m \nu_m$. This shift will later be eliminated after a polaron transformation (see Appendix A for more details).

Collective electronic excitations - Dipole-dipole exchanges at rates $\Omega_{jj'}$ have a strong imprint at nm distances, owing to their scaling with the inverse cube of the particle separation $|\vec{r}_j - \vec{r}_{j'}|^{-3}$ in the near field region [9]. This can be listed in the Hamiltonian as

$$\mathcal{H}_{\text{d-d}} = \sum_{j \neq j'} \Omega_{jj'} \sigma_j^\dagger \sigma_{j'} \quad (2)$$

and describes an excitation transfer between pairs of monomers via a virtual photon exchange. The coherent exchange is mediated by the dipole-dipole frequency shifts $\Omega_{jj'}$, which in units of the optical emission rate γ_0 are given by $\Omega_{jj'}/\gamma_0 = -3\pi/k_0 \vec{\mu}^* \cdot \text{Re } \mathbf{G}(\vec{r}_j, \vec{r}_{j'}, \omega_0) \cdot \vec{\mu}$, namely, proportional to the real part of the Green's tensor in free space (see Appendix B). In the following we will consider the particular case of side-by-side arrangement, where all transition dipoles $\vec{\mu}$ are parallel to each other and perpendicular to the chain direction.

Radiative and vibrational loss - In a master equation formulation for the system density operator ρ written as $\partial_t \rho = i[\rho, \mathcal{H}] + \mathcal{L}[\rho]$ loss can be included via the Lindblad superoperator $\mathcal{L}_\gamma[\rho] = \gamma_0/2 [2\mathcal{O}\rho(t)\mathcal{O}^\dagger - \mathcal{O}^\dagger\mathcal{O}\rho(t) - \rho(t)\mathcal{O}^\dagger\mathcal{O}]$, describing decay at generic rate γ_0 through a single channel with a generic collapse operator \mathcal{O} . For vibrational loss, the collapse rate for each mode m is Γ_m and the corresponding collapse operator is $b_{jm} - \sqrt{s_m} \sigma_j^\dagger \sigma_j$. This form for the collapse operator is derived in analogy to the dissipative physics of optomechanical systems in the ultra-strong coupling regime [21]. The radiative loss is not in diagonal Lindblad form but achieves the following expression $\mathcal{L}_e[\rho] = \sum_{j,j'} \gamma_{jj'}/2 [2\sigma_j \rho \sigma_{j'}^\dagger - \sigma_{j'}^\dagger \sigma_j \rho - \rho \sigma_{j'}^\dagger \sigma_j]$. This form can be diagonalized and it shows the emergence of \mathcal{N} independent decay channels, each corresponding to some collective electronic superposition state [9]. At very small separation, deep into the subwavelength regime, the fully symmetric superposition decays at a superradiant rate roughly equal to $\mathcal{N}\gamma_0$ while all other states have vanishingly small decay rates (which we will assume in the following to be exactly zero). This is by no means a limitation of our treatment as one can easily generalize this to the case of non-zero decay rates of the dark manifold [9, 20].

Collective basis formulation - The model can be better tackled in the collective basis, as has been previously considered in Ref. [20]. In the mesoscopic limit, where \mathcal{N}

is very large, the system illustrated in Fig. 1(a) can be considered translationally invariant and periodic boundary conditions can be invoked. Furthermore, in the deep subwavelength regime where $k_0 d \ll 1$, the eigenstates of the Hamiltonian in Eq. (2) are collective excitation states. A single symmetric mode can be distinguished with state vector obtained by the application of the symmetric operator $\mathcal{S}^\dagger = \sum_j \sigma_j^\dagger / \sqrt{\mathcal{N}}$ to the collective ground state. To a good approximation the system can be considered to be in the Dicke limit where a single superradiant emission rate roughly estimated by $\gamma_S = \mathcal{N}\gamma_0$ characterizes this 'bright' state. In addition, the other orthogonal $\mathcal{N} - 1$ asymmetric states are obtained via the application of asymmetric operators $\mathcal{A}_q = \sum_{j=1}^{\mathcal{N}} e^{iqjd} \sigma_j / \sqrt{\mathcal{N}}$ indexed by the quasi-momentum $q = 2\pi k / (\mathcal{N}d)$ obtained by a rescaling of the index of the mode $k = \pm 1, \dots, \pm(\mathcal{N} - 1)/2$ as used in Ref. [20] (for simplicity of notations, we restrict the discussion here to the \mathcal{N} odd case). These states are non-radiative at such deep subwavelength molecular separations and we dub them therefore as 'dark' as they are situated outside the light cone.

The collective excitations are eigenstates of the dipole-dipole interaction Hamiltonian

$$\mathcal{H}_{\text{d-d}} \mathcal{A}_q |g\rangle^{\otimes \mathcal{N}} = \Omega_q \mathcal{A}_q |g\rangle^{\otimes \mathcal{N}}, \quad (3)$$

where by definition we fix the symmetric shift $\Omega_S \equiv \Omega_{q=0}$. With periodic boundary conditions imposed, in the mesoscopic limit, one can derive the collective shifts as $\Omega_q = 2 \sum_j \Omega_{1j} \cos(q(j-1)d)$ [14, 20]. Further simplifications occur by considering the nearest neighbour approximation and the collective eigenenergies become $\Omega_q = 2\Omega \cos(qd)$, where the nearest-neighbour coupling is simply denoted by $\Omega \equiv \Omega_{12}$. The dipole-dipole Hamiltonian can now be recast in terms of the collective operators in the single excitation subspace

$$\mathcal{H}_{\text{d-d}} = \Omega_S \mathcal{S}^\dagger \mathcal{S} + \sum_{q \neq 0} \Omega_q \mathcal{A}_q^\dagger \mathcal{A}_q \quad (4)$$

which is derived by using the orthonormality condition $\sum_q e^{iqd(j-j')} = \mathcal{N} \delta_{jj'}$. Closely following the procedure introduced in Ref. [20], one can analyze the coupling between states of different symmetries via electron-vibron couplings by an additional transformation to a collective basis for the vibrational degrees of freedom as well. This is done by introducing collective vibrational modes $Q_q^{(m)} = \sum_{j=1}^{\mathcal{N}} (b_{m,j} + b_{m,j}^\dagger) e^{iqjd} / \sqrt{\mathcal{N}}$, with the momentum quadratures satisfying $[Q_q^{(m)}, P_q^{(m)}] = i$ and m labels the vibrational mode running from 1 to n . The Hamiltonian coupling the symmetric state to the dark state manifold is then given by

$$\mathcal{H}_{\text{int}}^{SA} = - \sum_{m=1}^n \sum_{q \neq 0} \frac{\sqrt{s_m} \nu_m}{\sqrt{\mathcal{N}}} \left(Q_q^{(m)} \mathcal{S}^\dagger \mathcal{A}_q + \text{h.c.} \right), \quad (5)$$

via collective vibrations. This coupling is responsible for funneling population into the long lived dark state manifold after the initial driving of the fully symmetric state

under uniform illumination. This mechanism is fundamental to understand the dynamics associated with Kasha's rule which we tackle in Sec. III. In addition, within the dark state manifold an all-to-all coupling Hamiltonian acts with the following form

$$\mathcal{H}_{\text{int}}^{\text{AA}} = - \sum_{m=1}^n \sum_{q \neq q'} \frac{\sqrt{s_m} \nu_m}{\sqrt{\mathcal{N}}} \left(Q_{q-q'}^{(m)} \mathcal{A}_q^\dagger \mathcal{A}_{q'} + \text{h.c.} \right), \quad (6)$$

and the sum implies that $q, q' \neq 0$. This indicates that a redistribution of energy takes place within the whole manifold of dark states. After transforming the system Hamiltonian, the energies of the collective states are shifted by the contribution of the symmetric vibrational mode $-\sum_m \sqrt{s_m} \nu_m Q_0^{(m)} / \sqrt{\mathcal{N}}$. The energy shifts can be removed by the collective polaron transformation $U = \prod_q \prod_{m=1}^n e^{i\sqrt{s_m}/\sqrt{\mathcal{N}} P_0^{(m)} \mathcal{A}_q^\dagger \mathcal{A}_q}$ which leads to a renormalization of the collective state energies as $\bar{\omega}_q = \omega_0 + \sum_m s_m \nu_m / 2 + \Omega_q$.

III. PHOTOPHYSICS OF J- AND H-AGGREGATES

The crucial point in analyzing the photophysics of aggregates is their small dimension and the very small monomer-monomer separation with respect to the incoming optical excitation wavelength. This means that laser driving takes place by the excitation of the symmetric collective mode which leads to a rescaling of the Rabi driving with a factor of $\sqrt{\mathcal{N}}$: this can be seen equivalently as an increase of the oscillator strength by $\sqrt{\mathcal{N}}$, thus rendering aggregates of any kind as good candidates for strong light-matter coupling. In addition, the particularity of the subsequent aggregate electronic dynamics lies within the shape of the energy band. For example, J-aggregates present an energy band where the symmetric mode at $q = 0$ lies at the bottom of the band thus leading to a bathochromic frequency shift (to the left of the bare monomer frequency) and subsequently shows not only an enhanced absorption cross section but also enhanced fluorescence at a superradiant rate. In contrast, H-aggregates have the symmetric state located at the top of the energy band corresponding to a hypsochromic shift (to the right of the monomer bare frequency, see Fig. 2(c)). Most importantly, quick dynamics follows the optical excitation involving the relaxation of the collective state towards low energy dark states. This takes place owing to the Hamiltonian in Eq. (5) which couples the symmetric state to the manifold of asymmetric states via vibrational Huang-Rhys factors and which is followed by quick vibrational relaxation.

Analytical results. Rate equations. - Let us now derive an analytical expression for the timescale associated with Kasha's rule, for the relaxation of the collective symmetric state. We largely follow the derivation in Ref. [20]

which we generalize here to incorporate the crucial aspect that many vibrational modes have to be taken into account. Under the assumption that the vibrational relaxation rates are fast compared to the coherent couplings and radiative loss rates, a set of rate equations for the populations of the symmetric state $p_S = \langle \mathcal{S}^\dagger \mathcal{S} \rangle$ and all dark states $p_q = \langle \mathcal{A}_q^\dagger \mathcal{A}_q \rangle$ can be derived (see Appendix C for more details). The intermediate step is the tracing out the vibrational modes as introduced in Ref. [20] and illustrated in Fig. 2(a). With the definitions κ_S - total loss rate of the symmetric state, κ_q - loss rate for dark state q , $\kappa_{q \rightarrow S}$ - incoherent repopulation rate from the dark to the bright state and $\kappa_{q' \rightarrow q}$ - incoherent rate for redistribution of energy within the dark state manifold, one can write

$$\dot{p}_S = -(\gamma_S + \kappa_S) p_S + \sum_{q \neq 0} \kappa_{q \rightarrow S} p_q, \quad (7a)$$

$$\dot{p}_q = -\kappa_q p_q + \sum_{q' \neq q} \kappa_{q' \rightarrow q} p_{q'}. \quad (7b)$$

The rate equations show that the symmetric state energy spills into the whole dark state manifold via rate κ_S and in addition, higher energy dark states spill into the lower energy ones via κ_q . The quasi-unidirectionality of the process is ensured by the fact that, in this perturbative treatment, the coherent coupling between states is followed by quick vibrational relaxation, making the reverse process, governed by rates $\kappa_{q \rightarrow S}$ and $\kappa_{q' \rightarrow q}$ from lower energy state to higher ones, very unlikely (as shown in Ref. [20] for the two monomer case). Mathematically, the condition is $\sqrt{s_m} \nu_m / \sqrt{\mathcal{N}} \ll \Gamma$. Analytically, one can get an expression for the transfer rate between the symmetric mode and any dark mode q mediated by vibrational mode m as

$$\kappa_{S \rightarrow q}^{(m)} = \frac{2s_m \nu_m^2 (\Gamma_m + \gamma_S) / \mathcal{N}}{(\Gamma_m + \gamma_S)^2 + 4(\Omega_S - \Omega_q - \nu_m)^2} \quad (8)$$

and construct the total rate to all states spanned by the index q by summing $\kappa_S = \sum_{m=1}^{n_{\text{max}}} \sum_q \kappa_{S \rightarrow q}^{(m)}$ over all vibrations up to an index n_{max} within the frequency interval covered by 4Ω where the electronic collective states are positioned in energy. Moreover, we will consider the standard underdamped harmonic oscillator model for the molecular vibrations, i.e. the dissipation rate is much smaller than the resonance frequency for any mode $\Gamma_m \ll \nu_m$. Equivalently, one can state that the quality factor of any vibrational mode is much larger than unity $\nu_m / \Gamma_m \gg 1$.

In order to further proceed with analytical estimates, let us first make some comments regarding typical timescales. Given that vibrational relaxation is in the order of tens to hundreds of GHz while spontaneous emission is in the range of tens of MHz, a very quick non-radiative path from the symmetric to low energy asymmetric states can be achieved on ps timescales. For monomer separations in the nm range, expected near field shifts Ω in the range of 1 THz to tens of THz are expected. This means that only a

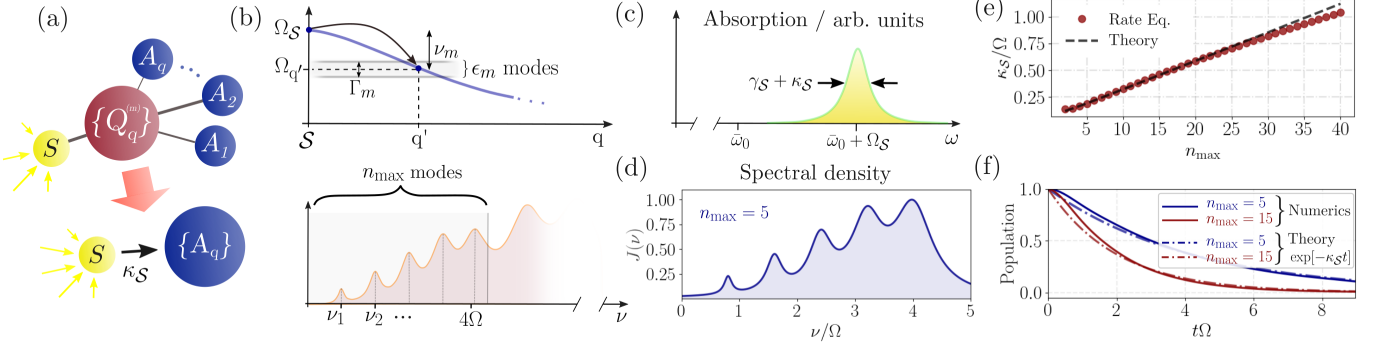


FIG. 2. (a) The initially excited symmetric mode is linked to all asymmetric modes via collective vibrational modes $Q_q^{(m)}$. Elimination of the vibrational degrees of freedom reveals a unidirectional transfer of energy into the dark state manifold. (b) Diagram illustrating the transfer $S \rightarrow q'$ into a number ϵ_m of asymmetric states located around a vibrational resonance ν_m (top). (Bottom) Only a limited number of vibrational modes, from 1 to n_{\max} can efficiently mediate resonant transfer between the symmetric state and the dark manifold. These modes are within the 4Ω bandwidth. (c) Absorption profile of a H-aggregate, exhibiting a hypsochromic frequency shift to the right of the monomer resonance. (d) Vibrational spectral density for equidistantly spaced vibrational frequencies ν_m , with identical Huang-Rhys factors $s = 0.01$ and relaxation rates $\Gamma_m = \nu_m/10$. (e) Linear scaling of the transfer rate κ_S as a function of the number of vibrational modes, with the same parameters as in (d) and $\mathcal{N} = 20$ molecules at $k_0 d = 0.0126$ separation. The scaling law from Eq. (11) provides a very good fit to the rate equations in Eq. (8). (f) Time dynamics of 20 molecules initialized in the symmetric state. Numerical results in the single excitation manifold show excellent agreement with an exponential decay given by $e^{-\kappa_S t}$, and governed by the analytical formula in Eq. (11) (Same parameters as in (d)-(e)).

few, low energy, molecular vibrations can fit in the window of 4Ω (see Fig. 2(b), bottom) and aid the relaxation process. This allows us to derive an approximate scaling law for κ_S as a function of a given number of vibrational modes n_{\max} that can efficiently mediate the relaxation of the symmetric state into the dark state manifold.

We proceed by first consider a given vibrational mode m and asking for the condition that this mode can transfer excitation from the symmetric mode to any of the dark states. This procedure is illustrated in Fig. 2(b) (top). We notice that with the condition that $\Gamma_m \ll \nu_m$ (it is also implied that $\gamma_S \ll \nu_m$ even for large \mathcal{N}) the resonance condition requires that the states to which resonant transfer can take place are only in the vicinity of the mode q fulfilling $\Omega_q = \Omega_S - \nu_m$. Of course, in this case one can immediately observe that any modes with $\nu_m > 4\Omega$ cannot take part in this transfer. Assuming a constant density of all \mathcal{N} collective states spread within the interval 4Ω , we can then estimate that a number of approximately $\epsilon_m = \Gamma_m \mathcal{N} / (4\Omega)$ states fall close to the resonance $\Omega_q = \Omega_S - \nu_m$, i.e. within the linewidth Γ_m . Summing over all these contributions gives the total rate for all transitions mediated by mode m to states close to q as

$$\sum_q \kappa_{S \rightarrow q}^{(m)} \approx \frac{\epsilon_m}{\mathcal{N}} \frac{2s_m \nu_m^2}{(\Gamma_m + \gamma_S)}. \quad (9)$$

The next step is the summation over all possible relaxation paths that participate in the transfer giving thus an estimate for the total rate

$$\kappa_S \approx \sum_{m=1}^{n_{\max}} \frac{\Gamma_m}{2\Omega} \frac{s_m \nu_m^2}{(\Gamma_m + \gamma_S)}. \quad (10)$$

In order to estimate the sum above, knowledge of the particular nature of the monomer's frequencies, Huang-Rhys factors and vibrational relaxation rates is necessary. However, while later we will numerically investigate random distributions of frequencies and Huang-Rhys factors, we aim first at deriving a simple scaling law. To this end we will proceed by making some simplifying assumptions, among which the first is that the vibrational spectrum is equally spaced in the interval from 0 up to 4Ω . We denote the frequency of mode m by $\nu_m = m4\Omega/n_{\max}$. Let us also consider that all Huang-Rhys factors are equal to s (later we compare with a randomized distribution with an average s). Moreover, we neglect the contribution of γ_S as it is much smaller than Γ_m (this should be typically very well fulfilled as γ_0/Γ_m is expected to be around 10^{-5}).

Summing over all vibrational modes within the interval of 4Ω gives us an approximated scaling law

$$\kappa_S \approx \frac{4s\Omega}{3} \frac{(n_{\max} + 1)(2n_{\max} + 1)}{n_{\max}}. \quad (11)$$

The result shows independence of the total number of monomers \mathcal{N} and a quasi linear dependence on the total number of available low frequency vibrational modes which can resonantly participate in Kasha's relaxation process from the high energy symmetric state to the bottom of the dark state manifold. Notice that the predicted timescale is dictated by the nearest neighbor dipole-dipole coupling strength Ω which in turn depends on the inverse cube of the monomer-monomer separation. In a first step, we can estimate that the analytical scaling is in very good agreement with the results of the rate equations, as seen in Fig. 2(e). The distribution of vibrational modes and their spectral density is shown in

Fig. 2(d). However, the important test of validity will be performed against numerical simulations of the full Hamiltonian and loss processes.

Comparison to numerics - The previously derived rate equations are obtained in the limit where the quickest timescale in the system is set by the rates Γ_m and for smaller than unity Huang-Rhys factors. The validity of this approach can be easily checked against numerical simulations restricted to the single excitation subspace of the total Hamiltonian in Eqs. (1) and (2). We therefore perform simulations in the single excitation subspace and follow the time evolution of the system assuming unit population of the symmetric state at the initial time $t = 0$. As Γ_m is larger than the coherent rates, any excitation of a vibration is followed by quick relaxation, justifying the assumption that any double excitation can be neglected.

The basis set is picked as a tensor product $|j\rangle \otimes |j'\rangle^{(m)}$ where by definition $|j\rangle = |g, g, \dots, e_j, \dots\rangle$ - only emitter j excited electronically and $|j'\rangle = |0, 0, \dots, 1_{j'}, \dots\rangle^{(m)}$ - only mode m in emitter j' has one vibrational excitation. Instead of solving the master equation directly, one can use the quantum jump formalism to evaluate single stochastic quantum trajectories using the Monte Carlo wave function method (MCWF). The advantage is that instead of describing the state of the quantum system by a density matrix of size $\mathcal{N}^4 \times n^2$ the stochastic method only requires state vectors of size $\mathcal{N}^2 \times n$. This is somewhat counteracted by the stochastic nature of the formalism which makes it necessary to repeat the simulation until the wanted accuracy is reached. However, in most scenarios, especially for higher dimensional quantum systems, the necessary number of repetitions is much smaller than the system size $\mathcal{N}^2 \times n$ and therefore using the MCWF method is advantageous (see Appendix D for more details). For the simulation we write

$$|\Psi\rangle = \sum_{j, j'=1}^{\mathcal{N}} \sum_{m=1}^n \alpha_{jj'}^{(m)} |g, g, \dots, e_j, \dots\rangle \otimes |0, 0, \dots, 1_{j'}, \dots\rangle^{(m)}, \quad (12)$$

with coefficients $\alpha_{jj'}^{(m)}$ and where the first part refers to the electronic excitation of molecule j and the second part to the excitation of the m -th vibrational mode of molecule j' .

In a first step, we compare the numerical results with the analytical scaling of Eq. (11), for an equidistant vibrational spectrum, in Fig. 2(f). A very good agreement is obtained showing that the time evolution of the symmetric state is well reproduced by an exponential decay following $e^{-\kappa_S t}$. In the next step we pick a set of randomly drawn vibrational frequencies $\nu_1, \dots, \nu_{n_{\max}}$ in the window 0 to 4Ω and Huang-Rhys factors $s_1, \dots, s_{n_{\max}}$ in the interval $[0, 0.2]$ (with an average $s = 0.1$). The results plotted in Fig. 3(a) show that a good fit is obtained with the simplified result of Eq. (11) which assumes evenly spaced vibrational frequencies and a Huang-Rhys factor at the level of the distribution

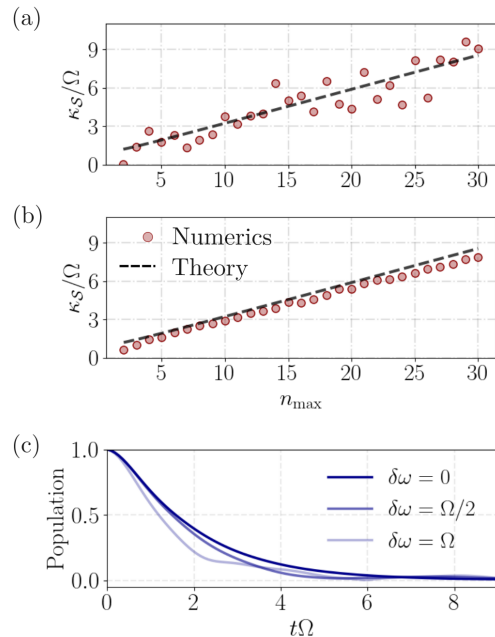


FIG. 3. (a) Numerical results for κ_S plotted against increasing n_{\max} for a randomly drawn set of vibrational frequencies $\nu_1, \dots, \nu_{n_{\max}}$ in the window 0 to 4Ω and Huang-Rhys factors $s_1, \dots, s_{n_{\max}}$ in the interval $[0, 0.2]$. The fit is performed with the analytical scaling in Eq. (11) for evenly spaced vibrational frequencies and Huang-Rhys factor at the level of the distribution average $s = 0.1$. (b) Further comparison of the analytical scaling from Eq. (11) with an average over 200 random realizations shows almost perfect agreement. (c) Decay of the initial symmetric state population under the influence of random static frequency disorder with fluctuation $\delta\omega$ around ω_0 . Further parameters in all plots: $\mathcal{N} = 20$ molecules, $k_0 d = 0.0126$, $\Gamma_m = \nu_m/10$, $\Omega \approx 3.759 \times 10^5 \gamma_0$.

average $s = 0.1$. Furthermore, an average of the numerical results over 200 random realizations predicts an excellent agreement to the linear fit predicted by Eq. (11).

Effects of frequency disorder - Let us now proceed with analyzing the effect of frequency disorder. As aggregates are immersed in solvents and usually under room temperature conditions, they are expected to present a large inhomogeneous broadening, at the level of THz. We consider a distribution of the \mathcal{N} monomer frequencies around ω_0 such that the frequency of each monomer becomes $\omega_0 + \delta_j$ where δ_j is randomly drawn from a distribution of width $\delta\omega$. In the collective basis, the symmetric state couples to any asymmetric state and acquires a shift as well [22]. The coupling of \mathcal{S} to a state q mediated by disorder is simply given by the Fourier transform of the distribution

$$\delta_q = \frac{1}{\sqrt{\mathcal{N}}} \sum_{j=1}^{\mathcal{N}} e^{iqj} \delta_j, \quad (13)$$

while the shift of the collective state $\delta_S = 1/\sqrt{\mathcal{N}} \sum_{j=1}^{\mathcal{N}} \delta_j$

is the average of the distribution, thus close to zero. According to Ref. [22], disorder induced couplings introduce an additional loss channel, thus slightly increasing the Kasha rate. This is indeed consistent with numerical simulations shown in Fig. 3(c) where the dynamics of the symmetric state without disorder and with considerable disorder at $\delta\omega = \Omega$ and $\delta\omega = 2\Omega$ are compared. The upshot is that the analytically derived loss rate holds well even for considerable disorder levels.

IV. CONCLUSIONS

Molecular aggregates are a perfect showcase of cooperative phenomena as their photophysics is naturally characterized by coherent and incoherent effects brought on by the positioning of individual monomers in the near field of each other. Effects widely explored in quantum optics, such as Dicke superradiance and subradiance, naturally occur in the theoretical description of such compounds, albeit in the presence of more complex, additional interactions between electrons and a vast number of molecular vibrations. We have provided a theoretical approach to the dynamics of collective electronic states making the connection, at the analytical and numerical level, with the physical mechanism introduced long ago by Kasha, stating that photon emission (fluorescence or phosphorescence)

occurs in appreciable yield only from the lowest excited state of a given multiplicity. Our analytical conclusions predict that the Kasha loss rate from the symmetric, high energy, optically addressable state to the lower energy states of an H-aggregate is roughly independent of the number of monomers but strongly dependent on the number of low energy vibrational modes which can be excited and then dissipate the accumulated energy afterwards.

Further investigations will focus on aspects such as the role of quantum coherence in such systems. An important direction is the application of the methods presented in this manuscript to photosynthetic systems under various conditions of illumination, ranging from spatially and time coherent laser light to spatially and time incoherent light sources.

Acknowledgments – We acknowledge financial support from the Max Planck Society and the Deutsche Forschungsgemeinschaft (DFG, German Research Foundation) – Project-ID 429529648 – TRR 306 QuCoLiMa (“Quantum Cooperativity of Light and Matter”). R. H. acknowledges funding from the Austrian Science Fund (FWF) doctoral college DK-ALM W1259-N27. We acknowledge fruitful discussions with Michael Reitz and Johannes Feist. The numerical simulations were performed with the open-source framework QuantumOptics.jl [23].

-
- [1] N. J. Hestand and F. C. Spano, “Expanded theory of H- and J-molecular aggregates: The effects of vibronic coupling and intermolecular charge transfer,” *Chemical Reviews* **118**, 7069–7163 (2018).
- [2] S. K. Saikin, A. Eisfeld, S. Valleau, and A. Aspuru-Guzik, “Photonics meets excitonics: natural and artificial molecular aggregates,” *Nanophotonics* **2**, 21–38 (2013).
- [3] S. Ma, S. Du, G. Pan, S. Dai, B. Xu, and W. Tian, “Organic molecular aggregates: From aggregation structure to emission property,” *Aggregate* **2**, e96 (2021).
- [4] D. Abramavicius, B. Palmieri, D. V. Voronine, F. Sanda, and S. Mukamel, “Coherent multidimensional optical spectroscopy of excitons in molecular aggregates; quasiparticle versus supermolecule perspectives,” *Chem. Rev.* **109**, 2350 (2009).
- [5] G. Scheibe, L. Kandler, and H. Ecker, “Polymerisation und polymere Adsorption als Ursache neuartiger Absorptionsbanden von organischen Farbstoffen,” *Naturwissenschaften* **25**, 75 (1937).
- [6] E. E. Jelley, “Spectral absorption and fluorescence of dyes in the molecular state,” *Nature* **138**, 1009 (1936).
- [7] M. Kasha, “Energy transfer mechanisms and the molecular exciton model for molecular aggregates(1, 2). 1963,” *Radiat. Res.* **178**, AV27–34 (1963).
- [8] F. J. Garcia-Vidal, C. Ciuti, and T. W. Ebbesen, “Manipulating matter by strong coupling to vacuum fields,” *Science* **373**, 6551 (2012).
- [9] M. Reitz, C. Sommer, and C. Genes, “Cooperative quantum phenomena in light-matter platforms,” *PRX Quantum* **3**, 010201 (2022).
- [10] R. H. Dicke, “Coherence in spontaneous radiation processes,” *Phys. Rev.* **93**, 99–110 (1954).
- [11] M. Gross and S. Haroche, “Superradiance: An essay on the theory of collective spontaneous emission,” *Physics Reports* **93**, 301 (1982).
- [12] G. Ferioli, A. Glicenstein, F. Robicheaux, R. T. Sutherland, A. Browaeys, and I. Ferrier-Barbut, “Laser-driven superradiant ensembles of two-level atoms near Dicke regime,” *Phys. Rev. Lett.* **127**, 243602 (2021).
- [13] P. Weiss, M. O. Araújo, R. Kaiser, and W. Guerin, “Subradiance and radiation trapping in cold atoms,” *New Journal of Physics* **20**, 063024 (2018).
- [14] A. Asenjo-Garcia, M. Moreno-Cardoner, A. Albrecht, H. J. Kimble, and D. E. Chang, “Exponential improvement in photon storage fidelities using subradiance and “selective radiance” in atomic arrays,” *Phys. Rev. X* **7**, 031024 (2017).
- [15] N. Killoran, S. F. Huelga, and M. B. Plenio, “Enhancing light-harvesting power with coherent vibrational interactions: A quantum heat engine picture,” *J. Chem. Phys.* **143**, 155102 (2015).
- [16] F. Caruso, A. W. Chin, A. Datta, S. F. Huelga, and M. B. Plenio, “Highly efficient energy excitation transfer in light-harvesting complexes: The fundamental role of noise-assisted transport,” *J. Chem. Phys.* **131**, 105106 (2009).
- [17] R. Holzinger, D. Plankensteiner, L. Ostermann, and H. Ritsch, “Nanoscale coherent light source,” *Phys. Rev. Lett.* **124**, 253603 (2020).
- [18] A. Mattioni, F. Caycedo-Soler, S. F. Huelga, and M. B.

- Plenio, “Design principles for long-range energy transfer at room temperature,” *Phys. Rev. X* **11**, 041003 (2021).
- [19] M. Reitz, C. Sommer, and C. Genes, “Langevin approach to quantum optics with molecules,” *Phys. Rev. Lett.* **122**, 203602 (2019).
- [20] R. Holzinger, S. A. Oh, M. Reitz, H. Ritsch, and C. Genes, “Cooperative subwavelength molecular quantum emitter arrays,” *Phys. Rev. Res.* **4**, 033116 (2022).
- [21] D. Hu, S.-Y. Huang, J.-Q. Liao, L. Tian, and H.-S. Goan, “Quantum coherence in ultrastrong optomechanics,” *Phys. Rev. A* **91**, 013812 (2015).
- [22] C. Sommer, M. Reitz, F. Mineo, and C. Genes, “Molecular polaritonics in dense mesoscopic disordered ensembles,” *Phys. Rev. Res.* **3**, 033141 (2021).
- [23] S. Krämer, D. Plankensteiner, L. Ostermann, and H. Ritsch, “Quantumoptics.jl: A Julia framework for simulating open quantum systems,” *Computer Physics Communications* **227**, 109 (2018).

Appendix A: Vibronic coupling

Let us justify the form of the Holstein Hamiltonian in Eq. (1) by following a first-principle derivation for a single nuclear coordinate R of effective mass μ . We assume that, along the nuclear coordinate, the equilibria for ground (coordinate R_g , state vector $|g\rangle$) and excited (coordinate R_e and state vector $|e\rangle$) electronic orbitals are different. Assuming equilibrium positions R_g and R_e for the potential surfaces of electronic ground and excited states, one can write the total molecular Hamiltonian describing both electronic and vibrational dynamics as

$$\mathcal{H}_{\text{mol}} = \left[\omega_0 + \frac{\hat{P}^2}{2\mu} + \frac{1}{2}\mu\nu^2 (\hat{R} - R_e)^2 \right] \sigma^\dagger \sigma + \left[\frac{\hat{P}^2}{2\mu} + \frac{1}{2}\mu\nu^2 (\hat{R} - R_g)^2 \right] \sigma \sigma^\dagger, \quad (\text{A1})$$

where μ is the reduced mass of the vibrational mode and $\sigma = |g\rangle\langle e|$. The kinetic and potential energies are written in terms of the position \hat{Q} and momentum operator \hat{P} describing the nuclear coordinate under consideration, with commutation $[\hat{Q}, \hat{P}] = i$. Introducing oscillations around the equilibria $\hat{Q} = \hat{R} - R_g$ and subsequently $\hat{R} - R_e = \hat{Q} + R_g - R_e =: \hat{Q} - R_{ge}$ we obtain

$$\mathcal{H}_{\text{mol}} = \frac{\hat{P}^2}{2\mu} + \frac{1}{2}\mu\nu^2 \hat{Q}^2 + \omega_0 \sigma^\dagger \sigma - \mu\nu^2 \hat{Q} R_{ge} \sigma^\dagger \sigma + \frac{1}{2}\mu\nu^2 R_{ge}^2 \sigma^\dagger \sigma. \quad (\text{A2})$$

We can now rewrite the momentum and position operators in terms of bosonic operators $\hat{Q} = q_{\text{zpm}}(b^\dagger + b)$, $\hat{P} = ip_{\text{zpm}}(b^\dagger - b)$. The bosonic operators satisfy the usual commutation relation $[b, b^\dagger] = 1$ and the zero-point motion displacement and momentum are defined as $q_{\text{zpm}} = 1/\sqrt{2\mu\nu}$ and $p_{\text{zpm}} = \sqrt{\mu\nu}/2$. Reexpressing the terms above yields the Holstein Hamiltonian

$$\mathcal{H}_{\text{mol}} = (\omega_0 + s\nu)\sigma^\dagger \sigma + \nu b^\dagger b - \sqrt{s\nu}(b^\dagger + b)\sigma^\dagger \sigma. \quad (\text{A3})$$

The dimensionless vibronic coupling strength s is given by $\sqrt{s} = \mu\nu R_{ge} q_{\text{zpm}}$ (s is called the Huang-Rhys factor and is typically on the order of $\sim 0.01 - 1$).

Appendix B: Vacuum mediated dipole-dipole coupling rates

The vacuum mediated dipole-dipole interactions for an electronic transition at wavelength λ_0 (corresponding wave vector $k_0 = 2\pi/\lambda_0$) between identical pairs of emitters separated by r_{ij} is given in terms of the free-space electromagnetic Green’s tensor $\mathbf{G}(\vec{r}_i - \vec{r}_j, \omega_0) \equiv \mathbf{G}(\vec{r}_{ij}, \omega_0)$, with $\vec{r}_{ij} = \vec{r}_i - \vec{r}_j$, which reads

$$\mathbf{G}(\vec{r}, \omega_0) = \frac{e^{ik_0 r}}{4\pi k_0^2 r^3} \left[(k_0^2 r^2 + ik_0 r - 1)\mathbb{I} + (-k_0^2 r^2 - 3ik_0 r + 3) \frac{\vec{r} \otimes \vec{r}}{r^2} \right], \quad (\text{B1})$$

where $r = |\vec{r}|$. The Green’s function $\mathbf{G}_{\alpha\beta}$ is a tensor quantity, with $\{\alpha, \beta\} = \{x, y, z\}$ which is determined by the polarization direction of the dipoles. In order to obtain the dipole-dipole couplings for H-aggregates we chose linear polarization in z -direction for all molecules, namely we take $\vec{\mu}_z^* \cdot \mathbf{G} \cdot \vec{\mu}_z$.

Appendix C: Deriving rate equations

Starting from the Holstein Hamiltonian in Eqs. (4)-(6) for \mathcal{N} identical molecules with n vibrational modes each. The Heisenberg equations for the collective electronic modes are given by

$$\dot{\mathcal{S}} = -i\left(\Omega_{\mathcal{S}} - \frac{\gamma_{\mathcal{S}}}{2}\right)\mathcal{S} + \frac{i\sqrt{s_m}\nu_m}{\sqrt{\mathcal{N}}} \sum_{m=1}^n \sum_q Q_q^{(m)} \mathcal{A}_q + \text{noise}, \quad (\text{C1a})$$

$$\dot{\mathcal{A}}_q = -i\Omega_q \mathcal{A}_q + \sum_{m=1}^n \frac{i\sqrt{s_m}\nu_m}{\sqrt{\mathcal{N}}} \left(Q_q^{(m)\dagger} \mathcal{S} + \sum_{q' \neq q} Q_{q-q'}^{(m)} \mathcal{A}_{q'} \right) + \text{noise}. \quad (\text{C1b})$$

The collective noise terms will be neglected from now on as they do not contribute to the transfer process.

To calculate the transfer rate from the symmetric state to the antisymmetric states we assume some initial population in the symmetric state and no population in the antisymmetric states, additionally we assume that the symmetric state decays independently and formally integrate

$$\mathcal{S}(t) = \mathcal{S}(0)e^{-(i\Omega_{\mathcal{S}} + \gamma_{\mathcal{S}}/2)t}, \quad (\text{C2a})$$

$$\mathcal{A}_q(t) = \mathcal{A}_q(0)e^{-i\Omega_q t} + \sum_{m=1}^n \frac{i\sqrt{s_m}\nu_m}{\sqrt{\mathcal{N}}} \int_0^t dt' e^{-i\Omega_q(t-t')} \left(Q_q^{(m)}(t') \mathcal{S}(t') + \sum_{q' \neq q} Q_{q-q'}^{(m)}(t') \mathcal{A}_{q'}(t') \right), \quad (\text{C2b})$$

and for the expectation value of the populations we get

$$\langle \dot{\mathcal{S}}^\dagger \mathcal{S} \rangle = -\gamma_{\mathcal{S}} \langle \mathcal{S}^\dagger \mathcal{S} \rangle - \sum_{m=1}^n \sum_q \frac{2\sqrt{s_m}\nu_m}{\sqrt{\mathcal{N}}} \text{Im} \langle \mathcal{S}^\dagger \mathcal{A}_q Q_q^{(m)} \rangle, \quad (\text{C3a})$$

$$\langle \dot{\mathcal{A}}_q^\dagger \mathcal{A}_q \rangle = - \sum_{m=1}^n \frac{2\sqrt{s_m}\nu_m}{\sqrt{\mathcal{N}}} \text{Im} \left(\langle \mathcal{A}_q^\dagger \mathcal{S} Q_q^{(m)} \rangle + \sum_{q' \neq q} \langle \mathcal{A}_q^\dagger \mathcal{A}_{q'} Q_{q'-q}^{(m)} \rangle \right). \quad (\text{C3b})$$

Therefore the terms $-2\sqrt{s_m}\nu_m/\sqrt{\mathcal{N}} \text{Im} \langle \mathcal{A}_q^\dagger \mathcal{S} Q_q^{(m)} \rangle$ will be responsible for population transfer from the symmetric to the antisymmetric state with quasi-momentum q at a rate $\kappa_{\mathcal{S} \rightarrow q}^{(m)}$. We can calculate the rates explicitly up to order $\mathcal{O}(s_m\nu_m^2)$ and assuming that correlations between vibronic and electronic operators factorize.

$$\begin{aligned} -2\sqrt{s_m}\nu_m/\sqrt{\mathcal{N}} \langle \mathcal{A}_q^\dagger \mathcal{S} Q_q^{(m)} \rangle &= -is_m\nu_m^2 \int_0^t dt' e^{-\Omega_q(t-t')} \langle Q_q^{(m)}(t') Q_q^{(m)}(t) \rangle \langle \mathcal{S}^\dagger(0) \mathcal{S}(0) \rangle e^{-\epsilon_S t'} e^{-\epsilon_S^* t} \\ &= -is_m\nu_m^2 \langle \mathcal{S}^\dagger(0) \mathcal{S}(0) \rangle \frac{e^{-\gamma_S t} - e^{-(\Gamma_m + \gamma_S)/2 + i(\Omega_S - \Omega_q - \nu_m)t}}{(\Gamma_m + \gamma_S)/2 + i(\Omega_S - \Omega_q - \nu_m)}, \end{aligned} \quad (\text{C4})$$

where we defined $\epsilon_S = -(\gamma_S/2 - i\Omega_S)$ and used the fact that different vibrational modes are uncorrelated at all times, i.e. $\langle Q_q^{(m')} (t') Q_q^{(m)} (t) \rangle = 0$ for $m' \neq m$. The correlations for $Q_q^{(m)}$ are evaluated assuming free evolution of the vibrations (to lowest order) and zero temperature for the vibrational modes:

$$\langle Q_q^{(m)}(t') Q_q^{(m)}(t) \rangle = \frac{1}{\mathcal{N}} \sum_{j=1}^{\mathcal{N}} \langle b_{jm}(t') b_{jm}^\dagger(t) \rangle = e^{-(\Gamma_m/2 - i\nu_m)(t-t')}. \quad (\text{C5})$$

The transfer rate can be written as

$$\kappa_{\mathcal{S} \rightarrow q}^{(m)} = \frac{2s_m\nu_m^2(\Gamma_m + \gamma_S)/\mathcal{N}}{(\Gamma_m + \gamma_S)^2 + 4(\Omega_S - \Omega_q - \nu_m)^2}, \quad (\text{C6})$$

given fast vibrational relaxation rates $\Gamma_m \gg \gamma_S$ compared to the electronic decay rates.

Appendix D: Single excitation subspace

The numerical diagonalization and subsequent time dynamics are evaluated in the single-excitation sector for both the electronic and vibrational degrees of freedom. This allows to rewrite the effective Hamiltonian in non-hermitian form as ($\hbar = 1$)

$$\mathcal{H}_{\text{eff}} = \sum_{j=1}^{\mathcal{N}} \left(h^{(j)} + \sum_{j'=1}^{\mathcal{N}} \left(\Omega_{jj'} - i \frac{\gamma_{jj'}}{2} \right) \sigma_j^\dagger \sigma_{j'} - \frac{i}{2} \sum_{m=1}^n \Gamma_m \mathcal{O}_{jm}^\dagger \mathcal{O}_{jm} \right), \quad (\text{D1})$$

where $h^{(j)}$ is defined in Eq. (1) and $\mathcal{O}_{jm} = b_{jm} - \sqrt{s_m} \sigma_j^\dagger \sigma_j$. The dynamics of the electron-vibron density matrix ρ can be described by a von Neumann equation of the form

$$i \frac{d}{dt} \rho(t) = [\mathcal{H}_{\text{eff}} \rho - \rho \mathcal{H}_{\text{eff}}], \quad (\text{D2})$$

and the expectation value of observable \mathcal{O} becomes $\bar{\mathcal{O}} = \text{tr}(\rho \mathcal{O})$. However, instead of solving the von Neumann equation directly, one can use the quantum jump formalism to evaluate single stochastic quantum trajectories using the Monte Carlo wave function method (MCWF). For large numbers of trajectories, the statistical average then approximates the result of the Master equation. The huge advantage is that instead of describing the state of the quantum system by a density matrix of size $\mathcal{N}^4 \times n^2$ these trajectories work in terms of state vectors of size $\mathcal{N}^2 \times n$. This is somewhat counteracted by the stochastic nature of the formalism which makes it necessary to repeat the simulation until the wanted accuracy is reached. It turns out, however, that for many cases, especially for high dimensional quantum systems, the necessary number of repetitions is much smaller than the system size $\mathcal{N}^2 \times n$ and therefore using the MCWF method is advantageous.

The system size stems from the fact, that in the single excitation subspace for both electronic and vibronic modes a general state vector can be written as

$$|\Psi\rangle = \sum_{j=1}^{\mathcal{N}} \alpha_{jj'}^{(m)} |g, g, \dots, e_j, \dots\rangle \otimes \sum_{m=1}^n \sum_{j'=1}^{\mathcal{N}} |0, 0, \dots, 1_{j'}, \dots\rangle^{(m)}, \quad (\text{D3})$$

with coefficients $\alpha_{jj'}^{(m)}$ and where the first part refers to the electronic excitation of molecule j and the second part to the excitation of the m -th vibrational mode of molecule j' . Thus, the single excitation assumption substantially reduces the Hilbert space dimension from $2^{\mathcal{N}} \times n_{\text{cut}}^{\mathcal{N}} \times n$ to $\mathcal{N}^2 \times n$ (where n_{cut} is the cut-off of the Fock space dimension for the vibrational modes), allowing the simulation of mesoscopic numbers of molecules.